Saudi Pharmaceutical Journal 28 (2020) 754–762

Contents lists available at ScienceDirect

Saudi Pharmaceutical Journal

journal homepage: www.sciencedirect.com

Original article

Intra-tumoral drug concentration mapping within solid tumor micro-milieu using in-vitro model and doxorubicin as a model drug

Ahmed M. Al-Abd [a,b,*], Alaa Khedr [c], Salah G. Atteiah [c,d], Fahad A. Al-Abbasi [e]

[a] Pharmacology Department, Medical Division, National Research Centre, Giza, Egypt
[b] Department of Pharmaceutical Sciences, College of Pharmacy, Gulf Medical University, Ajman, United Arab Emirates
[c] Faculty of Pharmacy, King Abdulaziz University, Jeddah, Saudi Arabia
[d] Faculty of Pharmacy, Zagazig University, Egypt
[e] Department of Biochemistry, Faculty of Science, King Abdulaziz University, Jeddah, Saudi Arabia

ARTICLE INFO

Article history:
Received 8 December 2019
Accepted 3 May 2020
Available online 11 May 2020

Keywords:
Solid tumors
Intratumoral pharmacokinetics
Spatial intratumoral drug distribution
Multicellular layers

ABSTRACT

In contrast to plasma pharmacokinetics, intratumoral pharmacokinetics of doxorubicin (DOX) determines its spatial anti-tumoral activity. Three-dimensional multicellular layers (MCL) model for solid tumors present optimum experimental platform for studying the intratumoral pharmacokinetics of DOX. This might imply new insights for understanding intratumoral pharmacokinetic parameters with realistic clinical implications. Herein, we are presenting simplified method for the spatial *in-situ* concentration assessment of DOX within the avascular simulating MCL solid tumor model of DLD-1 and HT-29 cell lines. DLD-1 and HT-29 formed viable well-structured MCL model abundant in extracellular matrix component (fibronectin). DOX (100 μM) showed stronger anti-proliferative effect against MCL of DLD-1 compared to HT-29 MCL (38.8% and 27.9%, respectively). The differential potencies of DOX closely correlate to the intratumoral pharmacokinetics within MCL's of both cell lines. DOX penetrated faster and washed out slower through the MCL of DLD-1 compared to HT-29 MCL. Distribution of DOX within MCL of DLD-1 was more homogenous compared to HT-29 MCL. Tissue concentration of DOX within MCL of DLD-1 was significantly higher than HT-29 MCL's after 96 h exposure (0.7 and 0.4 μmole/gm tissue, respectively). Concentration of DOX within MCL of both cell lines exceeded the IC_{50} under monolayer conditions (2.3 ± 0.6 μM and 0.6 ± 0.1 μM, respectively). In addition, DOX was extensively metabolized to less active metabolites (doxorubicinol and doxorubicinone) through the thickness of both MCL's. In conclusion, Intratumoral pharmacokinetic barriers to DOX might be key determinant in drug resistance on the tissue level, despite cellular and molecular events.

1. Introduction

Doxorubicin (DOX) is a cytotoxic anthracycline antibiotic originally isolated from *Streptomyces peucetius* var. *caesius* and has been used for more than three decades in the treatment of several malignancies. To the best of our knowledge, DOX is not included as a treatment option for colorectal cancer (Arcamone et al., 1969; Hortobagyi, 1997; Lown, 1993). This was attributed to the abundance of multidrug resistance and the expression of P-gp pump on most of the colorectal cancer cell lines (Shukla et al., 2011). Despite considering the cellular pharmacokinetics of DOX as potential factor of resistance (Al-Abd et al., 2013, 2011), multicellular resistance and avascular tissue penetration/distribution was obscured (Minchinton and Tannock, 2006; Tannock et al., 2002).

In contrast to plasma pharmacokinetics, intratumoral pharmacokinetics of DOX determines its spatial anti-tumoral activity. Yet, several drug delivery systems (DDS) and administration routes have been proposed for DOX to improve its tumoral delivery and decrease its distribution to normal non-tumoral tissues (Bagalkot et al., 2006; Gao et al., 2005; Weinberg et al., 2007). Most of the pharmacokinetics modules study DOX distribution till the point of enhanced permeation and retention (EPR) and/or total

* Corresponding author at: Department of Pharmacology, Medical Division, National Research Centre, Giza, Egypt.
E-mail address: ahmedmalabd@pharma.asu.edu.eg (A.M. Al-Abd).
Peer review under responsibility of King Saud University.

Production and hosting by Elsevier

https://doi.org/10.1016/j.jsps.2020.05.001

intratumoral distribution/accumulation relative to normal tissues (Al-Abd et al., 2010). As a matter of fact, it is quite complicated to study the spatial avascular distribution of anticancer drug *in-vivo* (Baker et al., 2008; Foehrenbacher et al., 2013). On the other hand, three dimensional culture models, such as multicellular layers (MCL), for solid tumors present optimum experimental platform for studying avascular pharmacokinetic parameters simulating the post-EPR micromilieu *in-situ* (Al-Abd et al., 2009b, 2008).

Studying the penetration of many anticancer drugs including DOX through MCL model has been repeatedly reported in the literature (Al-Abd et al., 2008; Hicks et al., 1998; Kyle et al., 2004). In addition, studying the avascular distribution of anticancer drugs within MCL model might imply new insights for understanding intratumoral pharmacokinetic parameters with realistic clinical implications. To the best of our knowledge, none of the previous studies assessed actual spatial drug concentration within MCL model. Instead, arbitrary fluorescent units were correlated to relative distance within MCL structure (Al-Abd et al., 2008; Kyle et al., 2004). This might be attributed to the difficulties in correlating microscopic derived signal (such as fluorescence intensity) and drug concentration *in-situ*.

Herein, we are presenting simplified mathematical method for the utilization of MCL solid tumor model in the spatial assessment for *in-situ* concentration mapping of a model drug (DOX) within avascular simulating condition.

2. Materials and methods

2.1. Chemicals and reagents

Doxorubicin hydrochloride and daunorubicin hydrochloride (internal standard) were purchased from Sigma Chemical Co. (St. Louis, MO, USA). Calcein-AM was purchased from Molecular Probes (Eugene, OR, USA). Cell culture reagents were purchased from Lonza group Ltd. (Basel, Switzerland); microporous membrane transwell inserts were purchased from Corning Costar (Acton, MA, USA). Heptanesulfonic acid sodium salt (HPLC-grade) was purchased from TCI Co. Ltd. (Tokyo, Japan). Acetone, $ZnSO_4$ and other reagents, including solvents, were of the highest analytical grade. Deionized water (18.2 MΩ, NANOpure diamond™, Brandstead water purification system, Fistreem International Co. Ltd. (Leicestershire, UK) was used throughout all HPLC analytical steps.

2.2. Cell culture

The human colorectal cancer cell lines, DLD-1 and HT-29, and bladder cancer cell lines were obtained from the ATCC (Huston, TX, USA) and maintained in RPMI-1640 media supplemented with 100 μg/mL streptomycin, 100 units/mL penicillin and 10% heat-inactivated fetal bovine serum. Cell cultures were kept in a humidified, 5% (v/v) CO_2 chamber at 37 °C.

2.3. Culture of cancer cells as multicellular layers (MCL)

MCL of cancer cells were grown as previously described [15]. Briefly, cells were grown on collagen-coated microporous membranes in Transwell inserts at a plating density of 1×10^6 cells/insert. The inserts were placed in a culture jar supplemented with suitable amount of media with continuous stirring in the bottom chamber. After 5 days of culture (MCL thickness of ~150 μm), each Transwell (n = 6) insert was transferred and assembled via size adaptor in a six-well plate containing 7 mL of media in the bottom of each well for subsequent drug and calcein-AM exposure. The culture jars as well as six-well plates were maintained in an incubator with a humidified atmosphere containing 5% CO_2 at 37 °C during the experiment.

2.4. Cytotoxicity assays

The cytotoxicity of DOX, was tested against DLD-1 and HT-29 cells by SRB assay as previously described [19]. Briefly, exponentially growing cells were harvested using 0.25% trypsin-EDTA and plated in 96-well plates at $2x10^3$ cells per well. Cells were exposed to DOX for 72 h and subsequently fixed with TCA (10%) for 1 h at 4 °C. After washings trice with distilled water, cells were exposed to 0.4% SRB solution for 10 min in dark place and subsequently washed with 1% glacial acetic acid. After drying overnight, tris-HCl (pH 7.4) was used to dissolve the SRB-stained cells and color intensity was measured at 540 nm using microplate reader (Skehan et al., 1990). Each concentration was repeated 6 times (n = 6) and the whole dose–response curve was replicated trice (n = 3).

2.5. Data analysis

The dose response curves of DOX were analyzed using E_{max} model (Eq. (1)).

$$\%\ \text{Cell viability} = (100 - R) \times \left(1 - \frac{[D]^m}{K_d{}^m + [D]^m}\right) + R \quad (1)$$

Where R is the residual unaffected fraction (the resistance fraction), [D] is the drug concentration used, K_d is the drug concentration that produces a 50% reduction of the maximum inhibition rate and m is a Hill-type coefficient. IC_{50} was defined as the drug concentration required to reduce color intensity to 50% of that of the control (i.e., $K_d = IC_{50}$ when R = 0 and E_{max} = 100-R) (Al-Abd et al., 2008).

2.6. Confocal microscopy

The integrity and vitality of MCL (n = 6) were assessed using confocal microscopy after staining with calcein-AM. Briefly, at the end of the culture period, calcein-AM was applied to the top chamber of the MCL at a final concentration of 4 μM and the MCL were then incubated at 37 °C for 30 min. MCL's were cut out of the Transwell insert, placed on a cover slip top side down and examined using a confocal laser scanning microscope (MRC 1024 MP; Bio-Rad, Hercules, CA, USA). Optical sections were acquired at 10-μm increments along the z-axis of the sample. Fluorescent images were obtained at $\lambda_{Ex/Em}$ = 488/517 nm and analyzed using Image-J ver. 1.47 (National Institute of Health, Bethesda, MD, USA).

2.7. Histological assessment for collagen and fibronectin contents within MCL

To make sure of tissue formation within MCL cultures, collagen and fibronectin contents were assessed histologicaly and immunohistologicaly, respectively as previously described [8]. Briefly, paraformaldhyde fixed MCL's (n = 3) were embedded in paraffin wax. Cross vertical sections (5 μm) were obtained and after dewaxing and rehydration, sections were stained with Masson's trichrome stain for collagen visualization. Another set of cross vertical sections (5 μm) were obtained and after dewaxing and rehydration, sections were incubated with 3% H_2O_2 for 30 min to eliminate the endogenous peroxidase activity. Nonspecific binding sites were blocked with normal donkey serum for 30 min and then incubated for 2 h at humidified chamber in mouse antiserum against fibronectin (dilution 1:100; Chemicon international Inc., Temecula, CA, USA). After rinsing in PBS, sections were incubated

in peroxidase-conjugated donkey anti-mouse IgG (dilution 1:200; Jackson ImmunoResearch Lab, Inc. West Grove, PA, USA) for 1 h. After washing, sections were incubated with a mixture of 0.05% 3,3′-diaminobenzidine containing 0.01% H_2O_2 at room temperature until a brown color was visible, and then washed with PBS, counterstained with hematoxylin, and mounted.

2.8. Fluorescent microscope signal calibration for DOX

To quantify DOX concentration within MCL after penetration, the microscopic acquired net fluorescent intensity (NFI) signals at $\lambda_{Ex/Em}$ = 482/505 were calibrated against serial DOX concentrations as follow. After growth for 5 days, MCLs (n = 6) were cut out of the transwells and 20 μm thick cross-horizontal frozen sections were obtained and mounted on glass slides. Fixed volume (1 μl) drops of serial DOX concentrations were applied on the horizontal sections and let to dry. The average greater and lesser diameters of each drop were measured microscopically, and the surface area was calculated. DOX exposed tissue volumes were calculated based on the surface area of each drop and section thickness (20 μm) and subsequently tissue weight was calculated according to tumor tissue specific density. Average NFI was plotted against DOX concentration and fitted using power equation best fit curve. NFI was obtained by bright field lens; direct light pass; incident light exposure time 1/30 sec.; and sensitivity grade 2 (400 dpi). Samples with NFI above or below limit of detection was re-measured at different incident light exposure time after recalibration. Average NFI was driven from 6 different fields per drops and total drops n = 3 for each DOX concentration (Weinberg et al., 2007).

2.9. Determining the avascular distribution of DOX using MCL model

To evaluate DOX avascular distribution kinetics, MCL's (n = 6) were exposed to DOX (100 μM) for a total of 96 h and fluorescent images of DOX within MCL structures were taken from cryosection at different time points as previously described (Al-Abd et al., 2008). Briefly, The MCLs were cut out of the Transwells and cross-vertical frozen sectioned (20 μm). A fluorescence microscope (AX70, TR-6A02; Olympus, Tokyo, Japan) was used to obtain fluorescent images at $\lambda_{Ex/Em}$ = 482/505 nm. Line morphometric analysis of fluorescent intensities from the top to the bottom layers of each MCL was performed using Optimas image analysis software. Data were corrected for tissue auto-fluorescence by subtracting it from the corresponding measurements and plotted against the distance from the surface layer of each MCL.

2.10. HPLC analysis for total depth DOX penetration and post penetration metabolism

Calibration curves for DOX in conditioned media were conducted to measure DOX concentrations after penetrating the full depth of MCL's. One hundred microliters of conditioned media was spiked with DOX calibration standards (3.4 nM to 344.8 nM); and incubated at 37 °C for 15 min to allow protein binding equilibrium. For protein precipitation, samples were vortex-mixed with 250 μl acetone and 100 μl ZnSO4 (saturated solution) and re-incubated at 37 °C for another 15 min. The supernatant was obtained after centrifugation and subjected to evaporation under a weak stream of nitrogen gas at room temperature. The dried residue was completely dissolved in 100 μl mobile phase and introduced into the HPLC system for analysis.

The HPLC system consisted of solvent delivery pump model-306, 231XL auto-sampler, and spectrofluorometric detector model-122 (Gilson Corp., Middleton, WI, USA). Reversed phase separation was performed on Luna™ analytical column (150 × 4.6 mm, C8, 5 μm, Phenomenex, Torrance, CA, USA) at room temperature. The mobile phase was a mixture of acetonitril: heptanesulfonic acid (0.2%, pH 4) at a ratio of 25:75, and the flow rate was set at 1.2 mL/min. Detection was performed at $\lambda_{ex/em}$ 482/550 nm. Peaks were recorded and integrated using UniPoint ver. 5.11 software (Gilson Corp., Middleton, WI, USA). Calibration curves were constructed using least squares regression method on the nominal concentration versus the peak height of DOX (Al-Abd et al., 2009a). At least three calibration curves were constructed with coefficients of variation (CV %) less than 15% at all nominal calibration concentrations and less than 25% at the lower limit of quantification (LOQ).

2.11. Characterization of DOX and its metabolites

Samples were analyzed by Agilent 1200 HPLC system (Agilent Technologies, Germany) consisting of a solvent delivery module, a quaternary pump, an autosampler, and a column compartment. The column effluent was connected to an Agilent 6320 Ion Trap LC-ESI-MS. The control of the HPLC system and data processing were performed using ChemStation (Rev. B.01.03 SR2 (204)) and 6300 Series Ion Trap Control version 6.2 Build no. 62.24 (Bruker Daltonik GmbH). The analytes were separated using Nucleodur C18ec column (150 × 4.6 mm, 100–5 μm) (Macherey-Nagel, Duren, Germany). Mobile system; A; 80% water, 10% methanol, 10% isopropanol, 0.05% ammonia solution (g/v), B; 20 isopropanol, 80% acetonitrile. Elution was isocratic 0 to 17 min with 100%A, then gradient elution at 17 to 20 min, to 60%A and 40%B.

The LC-IT-MS^2 spectrum of DOX and its metabolites are shown in Fig. S1. The fragmentation profile and product ions were matched with previous report (Wang et al., 2019).

2.12. Statistical analysis

Data are presented as the mean ± SEM. One way analysis of variance (ANOVA) followed by post hoc turkey test was used to examine the statistical significance of the data using SPSS® for windows, version 17.0.0., where $p < 0.05$ was considered statistically significant.

3. Results

3.1. Antiproliferative effect of DOX against monolayer and multicellular cultures of colorectal cancer cell lines

To simulate the intratumoral avascular micromilieu of solid tumor, two different colorectal cancer cell lines (DLD-1 and HT-29) were culture in three dimensional MCL culture as described in the methods section. MCL's of DLD-1 and HT-29 cells were cultured for 5 days to reach thickness of 144.8 ± 5.2 and 157.4 ± 3.4 μm, respectively (Fig. 1-E). DLD-1 and HT-29 cells within the avascular MCL structure were positive to calcein-AM staining and were found to be intervening in a tissue like structure (Fig. 1-A). This confirmed the viability of both cell lines within the avascular system of MCL. In addition and to confirm tissue formation, abundance of the extracellular matrix elements, collagen and fibronectin, was assessed histologically within the MCL's of both types of cells. Collagen within MCL's of both cell lines could not be visualized histologically after Masson's trichrome staining (Fig. 1-B). On the other hand, fibronectin was highly abundant in MCL's of both cell types (Fig. 1- C). MCL's of DLD-1 and HT-29 cells showed significant resistant to DOX compared to their monolayer culture. In MCL structure, the change in thickness was considered as indicator for the anti-proliferative effect of DOX (100 μM). In DLD-1, thickness of MCL's did not change significantly after 24 h

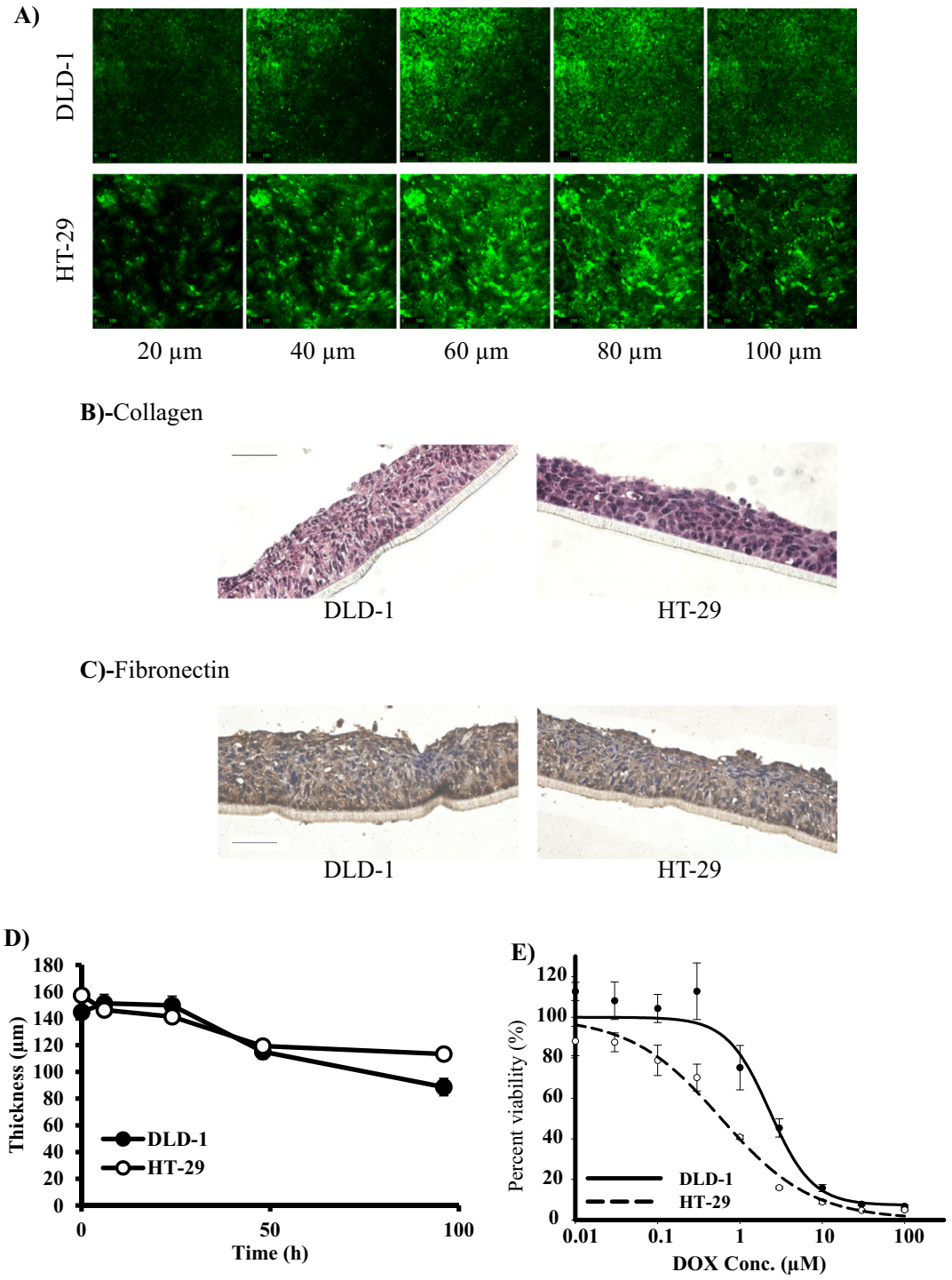

Fig. 1. Characterization of DLD-1 and HT-29 cell lines cultured as MCL's. Viability of cells was assessed by the viability probe, calcein-AM; images were produced by optical laser sectioning from top to bottom layers at 20 μm increment along the z-axis (A). Abundance of the extracellular matrix components, collagen (B) and fibronectin (C) were checked by histochemical techniques. Thickness of MCL's of both cell lines was followed up microscopically after treatment with DOX (100 μM) for up to 96 h (D); and compared to dose response curve of DOX against monolayer culture of both cell lines (E).

of exposure to DOX. After 48 h thickness of the MCL decreased to 115.1 ± 5.5 μm and further decreased to 88.6 ± 6.5 μm after 96 h of exposure. In HT-29, thickness of MCL's decreased gradually to 141.3 ± 2.6 and 119.3 ± 4.7 μm after 24 and 48 h of exposure, respectively (Fig. 1-D). no further significant change in the thickness of HT-29 MCL's was detected until 96 h. Collectively, it took 96 h for DOX (100 μM) to decrease the thicknesses of DLD-1 and HT-29 MCL's by only 38.8% and 27.9%, respectively. On the other hand, the IC_{50}'s (50% inhibition for proliferation) of DOX in monolayer cultures of DLD-1 and HT-29 cell lines were as low as 2.3 ± 0.6 μM and 0.6 ± 0.1 μM, respectively (Fig. 1-E).

3.2. Calibrating DOX concentration within MCL structure

To calculate the exact concentration of DOX within the avascular solid tumor micromilieu simulated by MCL culture, serial

concentrations of DOX were prepared per unit weight as described in the methods section and plotted against microscopically derived fluorescence intensities (NFI). Exposure of tissue to DOX induced increasing NFI in a concentration range of 1–100 μM (equivalent 3.4 to 440.4 nmole/gm tissue) (Fig. 2-A). The relationship between DOX concentration and NFI followed power function ($Y = aX^b$) within the upper and lower limits of quantifications with R^2 value of 0.8851. Exposure to DOX concentration higher than upper limit of quantification could not be assessed due to red fluorescence intensity saturation. Lower concentration than the lower limit of quantification could not be differentiated from tissue autofluorescence (Fig. 2-B). To extend the NFI with the range of quantification, time of incident fluorescent light was changed and recalibrated against the out-lying NFI values. The relationship between NFI and time of incident light was found to follow normal logarithmic relationship with R^2 value of 0.9353 (Fig. 2-C). Both calibration curves were used later on to calculate DOX concentration within MCL cultures.

3.3. Assessment of the avascular distribution of DOX using MCL model of colorectal cancer cells

The avascular distribution of DOX was assessed within MCL of DLD-1 and HT-29 cell lines after exposure to 100 μM for up to 96 h (Fig. 3). NFI derived from MCL cross sections was converted into concentration units (based on the previously mentioned calibration curves) and plotted against the spatial position within MCL geometry. Distance across MCL culture was calculated from surface (top layer) to bottom layers (membrane support). DOX distribution was found slower through MCL of HT-29 compared to DLD-1 cells. Fluorescent signal of DOX was confined to the top layers of MCL's of both cell lines until 3 h post exposure. Afterward, DOX penetrated throughout the whole body of DLD-1 MCL and distributed homogenously after 24 h. while DOX did not manage to distribute evenly through the MCL of HT-29 before 96 h. Obvious tissue destruction was observed particularly to the top layers of DLD-1 MCL (Fig. 3-A). This might be attributed to the high concentration and longer exposure duration to DOX in these top layers. Quantitatively, DOX could not reach deeper than 120, and 90 μm within MCL's of DLD-1 and HT-29, respectively until 3 h post exposure. During the first 3 h of exposure, DOX concentration within the top layers of MCL's did not exceed 1 μmole/gm tissue. After 6 h, DOX could penetrate throughout the whole depth of MCL's of both cell lines. However, DOX distribution was two folds higher in the top layers (until 85 μm depth) compared to bottom layers of both cell lines. After 24 h, DOX homogenously distributed amongst the whole depth of DLD-1 MCL reaching maximum concentration of 1.6 μmole/gm tissue at spatial depth of 21 μm from surface. On the other hand, DOX could not homogenously distribute within the MCL of HT-29 and accumulated in a spatial depth from 17 to 65 μm constituting DOX concentration higher than 0.7 μmole/gm tissue. Spatial distribution of DOX in layers deeper than 85 μm of HT-29 MCL's was found in concentration lower than 0.2 μmole/gm tissue. Distribution of DOX within the MCL's of DLD-1 after 48 h of exposure was found similar to that after 24 h with slightly lower DOX concentration in all spatial regions of MCL's (DOX concentration did not exceed 0.9 μmole/gm tissue). Profile of DOX distribution after 48 h within the MCL's of HT-29 was similar to that after 24 h with slightly higher DOX concentration in spatially deep layers. After 96 h, DOX concentration was homogenously distributed throughout the whole depth of MCL's of both cell lines; however, in significantly lower concentration compared to the previous time point. DOX concentration did not exceed 0.7 and 0.4 μmole/gm tissue within all spatial positions within MCL's of DLD-1 and HT-29, respectively (Fig. 3-B). We can conclude that DOX penetrated faster through the MCL of DLD-1 and was eliminated faster from the MCL of HT-29.

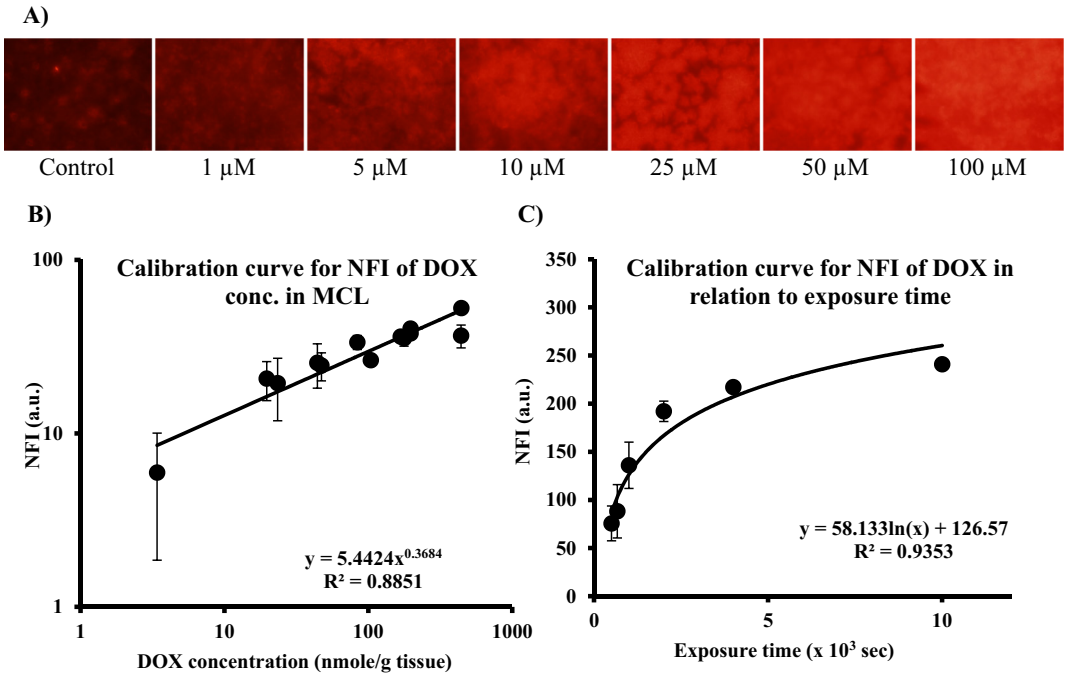

Fig. 2. Calibrating DOX concentration and microscopically derived fluorescent signal within MCL. Horizontal MCL sections (20 μm) of MCL were exposed to 1 μl of serial dilution of DOX concentration (Fig. 2-A). Diameter of DOX drop was calculated microscopically; DOX concentration per tissue mass was calculated and plotted against microscopically derived fluorescent intensity (NFI) at microscopic specifications: laser exposure 1/30 s; lens sensitivity 400 dpi (Fig. 2-B). NFI was further calibrated against different laser exposure times to expand the range of quantification (Fig. 2-C).

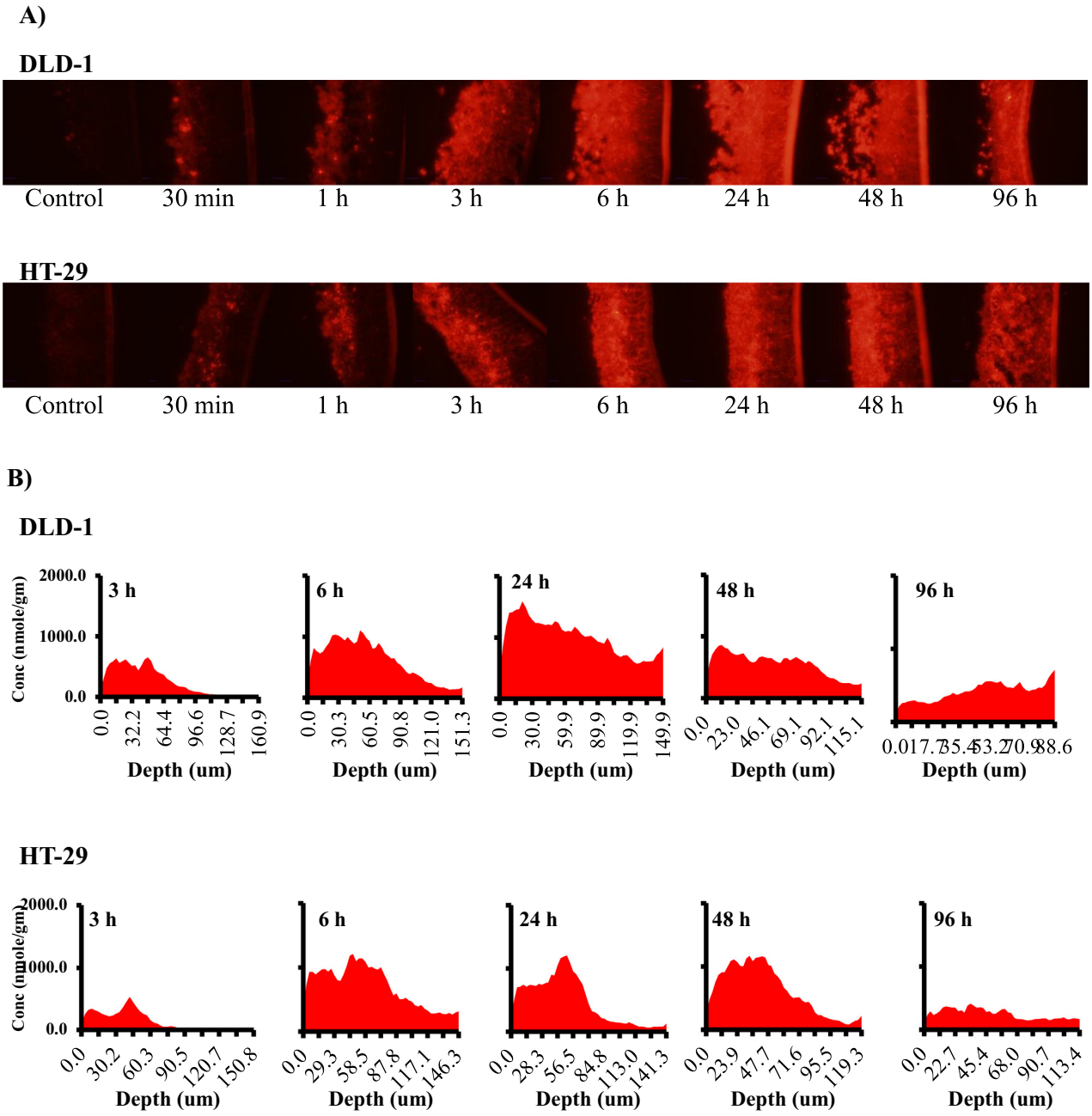

Fig. 3. Distribution profile of DOX within MCL's of DLD-1 and HT-29. MCL's were exposed to 100 μM DOX for up to 96 h and snap-frozen immediately at specific time points and cryo-sectioned for fluorescent imaging (Fig. 3-A). Microscopically derived DOX-induced NFI was converted into concentration units and distribution profile was plotted against spatial position within MCL (Fig. 3-B).

3.4. Determination of the post MCL penetration concentration of DOX and its related metabolites

To measure DOX concentration after traversing the full depth of DLD-1 and HT-29 MCL's, aliquots from the bottom treatment chambers were withdrawn at different time intervals and assayed by HPLC DOX concentration. DOX peak appeared at retention time (RT) of 12 min. Two DOX metabolites, M1 and M2 appeared at RT's 7 and 10 min, respectively (Fig. 4-A). Calibration curves (n = 3) for DOX were conducted in conditioned RPMI-1640 media with linearity range from 3.4 nM to 344.8 nM (Fig. 4-B). DOX could not be detected on the other face of both cell lines' MCL's before 6 h of exposure. After 6 h, DOX manage to penetrate the full depth of both DLD-1 and HT-29 MCL's showing concentration in the bottom chamber of 8.8 ± 0.3 and 6.9 ± 0.2 nM, respectively. After 24 h of exposure, post-penetration DOX concentration kept increasing through MCL's of DLD-1 and HT-29 reaching to 21.2 ± 2.1 and 25.4 ± 1.2 nM, respectively. After 48 h, post-penetration concentration of DOX through HT-29 MCL increased significantly to 70.1 ± 8.5 nM compared to 28.7 ± 1.7 nM through the MCL of DLD-1. Post-penetration DOX concentration decreased significantly after 96 h of exposure only in case of HT-29 MCL to 42.6 ± 1.7 nM; while kept increasing after penetration through DLD-1 MCL to reach 34.8 ± 2.1 nM (Fig. 4-C). DOX metabolites, M1 and M2 were characterized by LC/MS and identified to be doxorubicinol and doxorubicinone. M1 appeared earlier (after 24 h of exposure) and substantially in a higher concentration after penetrating MCL of HT-29 compared to MCL of DLD-1 (after 48 h of exposure). Concentrations of M1

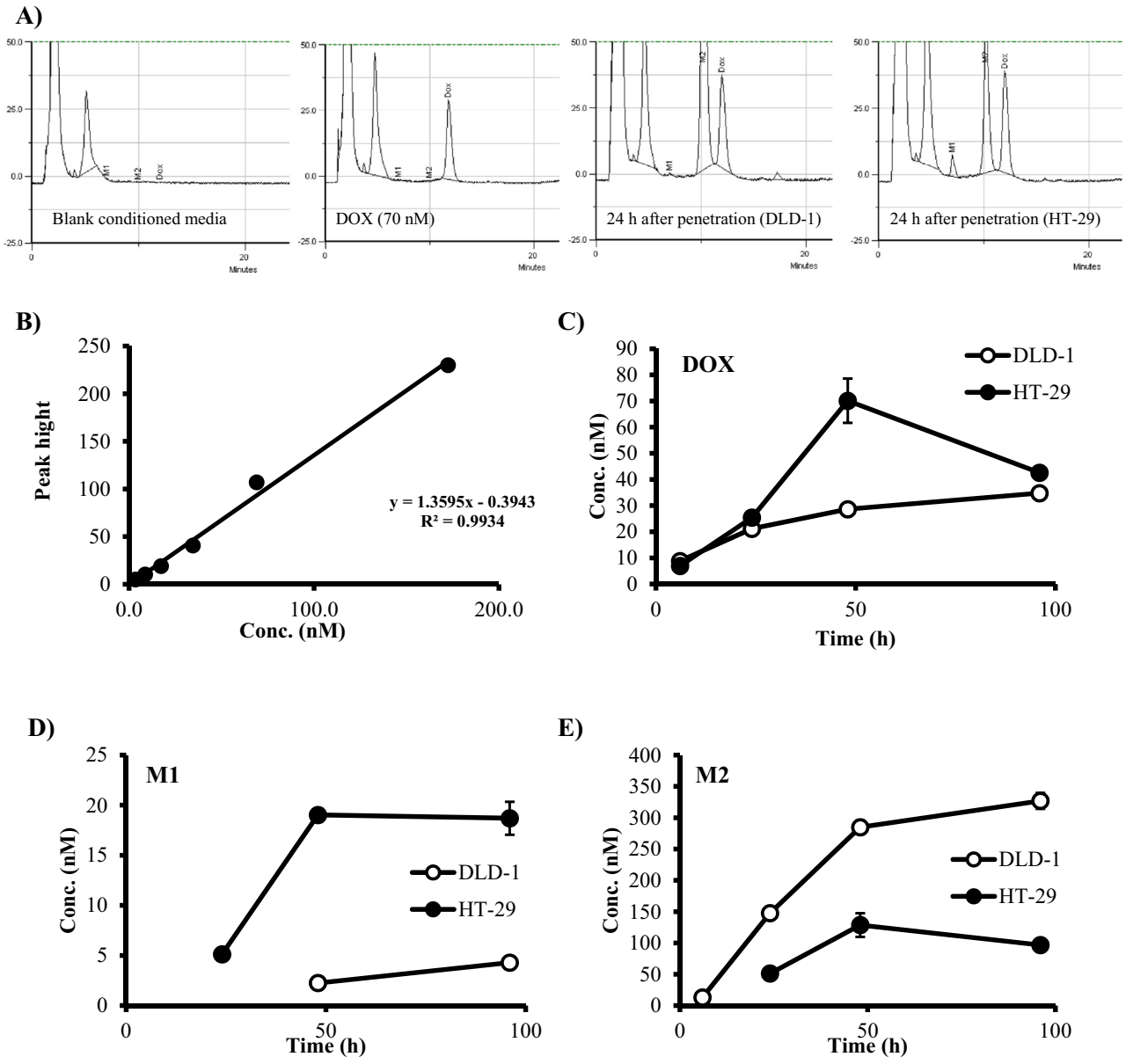

Fig. 4. Chromatographic assessment for DOX after penetrating the full thickness of DLD-1 and HT-29 MCL's. MCL's were exposed to DOX (100 μM) for up to 96 h; and samples from the bottom chamber were aliquoted and assayed for DOX and its major metabolites. Representative chromatograms for blank media, media spiked with DOX and media after 24 h treatment with DOX against MCL's of DLD-1 and HT-29 (Fig. 4-A). Calibration curve for DOX peak hight within conditioned media and used to calculate DOX concentration (Fig. 4-B). Concentration of DOX (Fig. 4-C), doxorubicinol (Fig. 4-D) and doxorubicinone (Fig. 4-E) were assayed in the bottom chamber after different time points of penetration.

after penetration through MCL of HT-29 were 5.1 ± 0.4 nM, 19.0 ± 0.2 nM and 18.7 ± 1.6 nM after 24 h, 48 h and 96 h respectively. However, concentrations of M1 after penetrating MCL of DLD-1 were 2.3 ± 0.2 nM and 4.3 ± 0.1 nM after 48 h and 96 h, respectively (Fig. 4-D). In contrast to M1, M2 appeared earlier (after 6 h) and substantially in higher concentration after penetrating MCL of DLD-1 compared to MCL of HT-29 (after 24 h). Concentrations of M2 after penetration through MCL of DLD-1 were 13 ± 0.4 nM, 147.8 ± 2 nM, 284.9 ± 11.4 nM and 327 ± 23.3 nM after 6 h, 24 h, 48 h and 96 h respectively. However, concentrations of M2 after penetrating MCL of HT-29 were 51.4 ± 2.6 nM, 128.7 ± 19 nM and 96.8 ± 6.6 nM after 24 h, 48 h and 96 h, respectively (Fig. 4-E). Collectively, the abundance of M2 metabolite after DOX penetration through the MCL's of both DLD-1 and HT-29 was significantly higher than M1.

4. Discussion

Resistance to chemotherapeutics might be attributed to molecular events at the cellular (Al-Abd et al., 2013) and sub-cellular levels (Mahmoud et al., 2012) or pharmacokinetic reasons at the whole body or localized tumor tissue levels (Kyle et al., 2007). In contrast to classic pharmacokinetics, intratumoral pharmacokinetics draw more accurate portfolio for chemotherapeutic drug distribution *in-situ*. Deriving such intratumoral pharmacokinetic parameters using *in-vivo* models is very complicated and suffers from huge ambiguity (Baker et al., 2008). Solid tumor microenvironment is considered avascular in nature; despite the high abundance of intratumoral blood vessels. This is attributed to the collapsed heterogeneous premature intratumoral vascular bed which is surrounded by crowded unorganized rapidly proliferating

tumor parenchyma. Several three-dimensional culture techniques are suggested to simulate the intratumoral micro-environmental traits in terms of drug penetration, distribution and efficacy. Herein, we used multicellular layers model of two colorectal cancer cell lines (DLD-1 and HT-29) to simulate the avascular solid tumor microenvironment in order to bring up intratumoral pharmacokinetic parameters for a model drug (doxorubicin). This might help in understanding colorectal cancer resistance to doxorubicin at the tissue level from the intratumoral pharmacokinetics point of view.

Fully compact and viable MCL's were formed from both cell lines (DLD-1 and HT-29) as visualized by the viability stain calcein-AM. Despite the actual thickness of MCL's exceeded 120 μm; viability could not be assessed deeper than 100 μm due to tissue induced photonic attenuation. This was previously reported in four different cell lines (HT-1376, J-82, DLD-1 and HT-29); in addition, penetration problem was noticed for calcein-AM and particularly in the MCL of DLD-1 cell line (Al-Abd et al., 2008). This might explain the weaker fluorescent signal within the MCL of DLD-1 compared to HT-29. MCL's of both cell lines formed tissue-like structure with abundant extracellular matrix component. It is known that some tumor cells can produce their own extracellular component such as collagen and fibronectin without co-culturing with fibroblast. This strengthen the three dimensional skeleton of these cell lines and facilitate their MCL culture formation (Tannock et al., 2002). Optimally, tumor tissue organoids might be more realistic intratumoral pharmacokinetics simulating *in-vitro* model (Devarasetty et al., 2018; Weeber et al., 2017). However, the irregular geometry of such model constitutes significant hurdle in front of mathematical modeling to derive pharmacokinetics parameters (Karolak et al., 2018). Both DLD-1 and HT-29 showed significantly higher resistance to DOX in MCL culture compared to the simplified monolayer culture. Interestingly, HT-29 cell line was more sensitive to DOX in monolayer culture while reciprocally, DLD-1 was more sensitive to DOX in MCL culture system. This differential response reflects the importance of the three-dimensional culture format in simulating the real solid tumor response *in-situ*. The differential response to chemotherapies of solid tumor cell line cultured in three dimensional versus monolayer culture system has been repeatedly mentioned in the literature (Al-Abd et al., 2008).

We and others believe that resistance to classic and modern anticancer drugs might be largely attributed to limited intratumoral pharmacokinetics and poor drug distribution (Al-Abd et al., 2009b, 2008; Grantab et al., 2006; Hicks et al., 1998; Kyle et al., 2007; Tannock et al., 2002). Spatial distribution of drugs within solid tumor micromilieu was assessed in the vast majority of previous studies in arbitrary or relative units (Al-Abd et al., 2009b, 2008). To the best of our knowledge, this is the first trial to portrait the avascular distribution of chemotherapeutic agents in real concentration units. In the current study, DOX was used as a proof of principle agent with known fluorescent properties and anticancer activity. The relationship between microscopically derived fluorescence signal of DOX and its tissue concentration follows power mathematical relationship; and the minimal effective DOX concentration in liver cancer should exceed 11 nmole/gm tissue (6.4 μg/gm tissue) *in-situ* (Weinberg et al., 2007). The calibration curve conducted in the current study covers far wider range of concentration (3.4 to 440 nmole/gm tissue) and could be expanded to higher concentration by modifying fluorescent beam specifications.

In the current study, DOX concentration within the MCL of both cell lines was found higher than 11 nmole/gm tissue for more than 72 h. However, the observed killing effect (decreased MCL thickness) was very limited. This correlates with the clinical resistance of colorectal cancer to anthracycline and particularly DOX (Comeau and Labruzzo Mohundro, 2013). This resistance was attributed to cell membrane related molecules such as P-gp efflux pump (Al-Abd et al., 2011) and sub-cellular molecular events such as micro-RNA molecules (miR-137) (Takwi et al., 2014). However, killing effect of DOX against DLD-1 and HT-29 cell lines were profoundly observed at concentration less than 5 nmole/ml after treatment for 72 h. From the pharmacokinetics point of view, full distribution and saturation of DLD-1 MCL with DOX was faster than MCL of HT-29 cells. In addition, DOX was eliminated from DLD-1 MCL in a slower rate than MCL of HT-29. Yet, this might carry pharmacokinetic explanation for the higher potency of DOX against DLD-1 MCL compared to MCL of HT-29. The slow distribution of DOX within MCL's of both cell lines was confirmed by analyzing the concentration of DOX after penetrating the full MCL thickness. No DOX appeared on the other side of the MCL before 6 h. DOX reaches its maximum concentration after 48 h in HT-29 MCL and declined thereafter. This might be attributed to the excessive metabolism rather than tissue binding. On the other hand, DOX concentration on the other side of DLD-1 MCL kept increasing steadily until 96 h this might be attributed to stronger tissue binding and slow dissociation from the MCL structure of DLD-1 on the top of excessive metabolism as well. Tissue binding is critical factor for avascular drug transport within solid tumor micro-region (Kuh et al., 1999; Toley et al., 2013). Resistance of some cell lines to DOX was attributed to its metabolism into doxorubicinol *in-situ* (Bains et al., 2013).

In conclusion, we suggested herein a method to quantify the intratumoral pharmacokinetic determinants of model drug (doxorubicin) within multicellular layers three-dimensional model of solid tumor. Intratumoral pharmacokinetic barriers might be key determinant in drug resistance on the tissue level, despite cellular and molecular levels.

Declaration of Competing Interest

The authors declare that they have no known competing financial interests or personal relationships that could have appeared to influence the work reported in this paper.

Acknowledgements

This paper was funded by the Deanship of Scientific Research (DSR), King Abdulaziz University, under grant No. (272/166/1434). The authors, therefore, acknowledge with thanks DSR technical and financial support. In addition, this work was partially funded by grant number (GMU/COP/GR/2019-10/004), Gulf Medical University, Ajman, UAE.

Appendix A. Supplementary data

Supplementary data to this article can be found online at https://doi.org/10.1016/j.jsps.2020.05.001.

References

Al-Abd, A.M., Al-Abbasi, F.A., Asaad, G.F., Abdel-Naim, A.B., 2013. Didox potentiates the cytotoxic profile of doxorubicin and protects from its cardiotoxicity. Eur. J. Pharmacol. 718. https://doi.org/10.1016/j.ejphar.2013.08.009.

Al-Abd, A.M., Hong, K.-Y., Song, S.-C., Kuh, H.-J., 2010. Pharmacokinetics of doxorubicin after intratumoral injection using a thermosensitive hydrogel in tumor-bearing mice. J. Control. Release 142. https://doi.org/10.1016/j.jconrel.2009.10.003.

Al-Abd, A.M., Kim, N.H., Song, S.-C., Lee, S.J., Kuh, H.-J., 2009a. A simple HPLC method for doxorubicin in plasma and tissues of nude mice. Arch. Pharm. Res. 32. https://doi.org/10.1007/s12272-009-1417-5.

Al-Abd, A.M., Lee, J.-H., Kim, S.Y., Kun, N., Kuh, H.-J., 2008. Novel application of multicellular layers culture for in situ evaluation of cytotoxicity and penetration of paclitaxel. Cancer Sci. 99. https://doi.org/10.1111/j.1349-7006.2007.00700.x.

Al-Abd, A.M., Lee, S.H., Kim, S.H., Cha, J.-H., Park, T.G., Lee, S.J., Kuh, H.-J., 2009b. Penetration and efficacy of VEGF siRNA using polyelectrolyte complex micelles in a human solid tumor model in-vitro. J. Control. Release 137. https://doi.org/10.1016/j.jconrel.2009.03.009.

Al-Abd, A.M., Mahmoud, A.M., El-Sherbiny, G.A., El-Moselhy, M.A., Nofal, S.M., El-Latif, H.A., El-Eraky, W.I., El-Shemy, H.A., 2011. Resveratrol enhances the cytotoxic profile of docetaxel and doxorubicin in solid tumour cell lines in vitro. Cell Prolif. 44, 591–601. https://doi.org/10.1111/j.1365-2184.2011.00783.x.

Arcamone, F., Cassinelli, G., Fantini, G., Grein, A., Orezzi, P., Pol, C., Spalla, C., 1969. Adriamycin, 14-hydroxydaunomycin, a new antitumor antibiotic from S. peucetius var. caesius. Biotechnol. Bioeng. 11, 1101–1110.

Bagalkot, V., Farokhzad, O.C., Langer, R., Jon, S., 2006. An aptamer-doxorubicin physical conjugate as a novel targeted drug-delivery platform. Angew. Chem. Int. Ed. Engl. 45, 8149–8152.

Bains, O.S., Szeitz, A., Lubieniecka, J.M., Cragg, G.E., Grigliatti, T.A., Riggs, K.W., Reid, R.E., 2013. A correlation between cytotoxicity and reductase-mediated metabolism in cell lines treated with doxorubicin and daunorubicin. J. Pharmacol. Exp. Ther. 347, 375–387. https://doi.org/10.1124/jpet.113.206805.

Baker, J.H., Lindquist, K.E., Huxham, L.A., Kyle, A.H., Sy, J.T., Minchinton, A.I., 2008. Direct visualization of heterogeneous extravascular distribution of trastuzumab in human epidermal growth factor receptor type 2 overexpressing xenografts. Clin. Cancer Res 14, 2171–2179. https://doi.org/14/7/2171 [pii]10.1158/1078-0432.CCR-07-4465.

Comeau, J.M., Labruzzo Mohundro, B., 2013. From bench to bedside: promising colon cancer clinical trials. Am. J. Manag. Care 19, SP32-7.

Devarasetty, M., Mazzocchi, A.R., Skardal, A., 2018. Applications of bioengineered 3D tissue and tumor organoids in drug development and precision medicine: Current and future. BioDrugs 32, 53–68.

Foehrenbacher, A., Secomb, T.W., Wilson, W.R., Hicks, K.O., 2013. Design of optimized hypoxia-activated prodrugs using pharmacokinetic/pharmacodynamic modeling. Front. Oncol. 3, 314. https://doi.org/10.3389/fonc.2013.00314.

Gao, Z.G., Lee, D.H., Kim, D.I., Bae, Y.H., 2005. Doxorubicin loaded pH-sensitive micelle targeting acidic extracellular pH of human ovarian A2780 tumor in mice. J. Drug Target 13, 391–397.

Grantab, R., Sivananthan, S., Tannock, I.F., 2006. The penetration of anticancer drugs through tumor tissue as a function of cellular adhesion and packing density of tumor cells. Cancer Res. 66, 1033–1039.

Hicks, Kevin O, Fleming, Yvette, Siim, Bronwyn G, Koch, Cameron J, Wilson, William R, 1998. Extravascular diffusion of tirapazamine: effect of metabolic consumption assessed using the multicellular layer model. Int. J. Radiat. Oncol.*Biol.*Phys. 42 (3), 641–649. https://doi.org/10.1016/S0360-3016(98)00268-5.

Hortobagyi, G.N., 1997. Anthracyclines in the treatment of cancer. An overview. Drugs 54 (Suppl 4), 1–7.

Karolak, A., Markov, D.A., McCawley, L.J., Rejniak, K.A., 2018. Towards personalized computational oncology: from spatial models of tumour spheroids, to organoids, to tissues. J. R. Soc. Interface 15, 20170703.

Kuh, H.J., Jang, S.H., Wientjes, M.G., Weaver, J.R., Au, J.L., 1999. Determinants of paclitaxel penetration and accumulation in human solid tumor. J. Pharmacol. Exp. Ther. 290, 871–880.

Kyle, A.H., Huxham, L.A., Chiam, A.S., Sim, D.H., Minchinton, A.I., 2004. Direct assessment of drug penetration into tissue using a novel application of three-dimensional cell culture. Cancer Res. 64, 6304–6309.

Kyle, A.H., Huxham, L.A., Yeoman, D.M., Minchinton, A.I., 2007. Limited tissue penetration of taxanes: a mechanism for resistance in solid tumors. Clin. Cancer Res. 13, 2804–2810.

Lown, J.W., 1993. Anthracycline and anthraquinone anticancer agents: current status and recent developments. Pharmacol. Ther. 60, 185–214.

Mahmoud, A.M., Al-Abd, A.M., Lightfoot, D.A., El-Shemy, H.A., 2012. Anti-cancer characteristics of mevinolin against three different solid tumor cell lines was not solely p53-dependent. J. Enzyme Inhib. Med. Chem. 27. https://doi.org/10.3109/14756366.2011.607446.

Minchinton, A.I., Tannock, I.F., 2006. Drug penetration in solid tumours. Nat. Rev. Cancer 6, 583–592.

Shukla, S., Ohnuma, S., V Ambudkar, S., 2011. Improving cancer chemotherapy with modulators of ABC drug transporters. Curr. Drug Targets 12, 621–630.

Skehan, P., Storeng, R., Scudiero, D., Monks, A., McMahon, J., Vistica, D., Warren, J.T., Bokesch, H., Kenney, S., Boyd, M.R., 1990. New colorimetric cytotoxicity assay for anticancer-drug screening. J. Natl. Cancer Inst. 82, 1107–1112.

Takwi, A.A., Wang, Y.M., Wu, J., Michaelis, M., Cinatl, J., Chen, T., 2014. miR-137 regulates the constitutive androstane receptor and modulates doxorubicin sensitivity in parental and doxorubicin-resistant neuroblastoma cells. Oncogene 33, 3717–3729. https://doi.org/10.1038/onc.2013.330.

Tannock, I.F., Lee, C.M., Tunggal, J.K., Cowan, D.S., Egorin, M.J., 2002. Limited penetration of anticancer drugs through tumor tissue: a potential cause of resistance of solid tumors to chemotherapy. Clin. Cancer Res. 8, 878–884.

Toley, B.J., Tropeano Lovatt, Z.G., Harrington, J.L., Forbes, N.S., 2013. Microfluidic technique to measure intratumoral transport and calculate drug efficacy shows that binding is essential for doxorubicin and release hampers Doxil. Integr. Biol. 5, 1184–1196. https://doi.org/10.1039/c3ib40021b.

Wang, X., Hui, R., Chen, Yun, Wang, W., Chen, Yujiao, Gong, X., Jin, J., 2019. Discovery of Novel Doxorubicin Metabolites in MCF7 Doxorubicin-Resistant Cells. Front. Pharmacol.

Weeber, F., Ooft, S.N., Dijkstra, K.K., Voest, E.E., 2017. Tumor organoids as a pre-clinical cancer model for drug discovery. Cell Chem. Biol. 24, 1092–1100.

Weinberg, B.D., Ai, H., Blanco, E., Anderson, J.M., Gao, J., 2007. Antitumor efficacy and local distribution of doxorubicin via intratumoral delivery from polymer millirods. J. Biomed. Mater. Res. A 81, 161–170.